Molecular Therapy
Nucleic Acids
Original Article

Combination of protein and cell internalization SELEX identifies a potential RNA therapeutic and delivery platform to treat EphA2-expressing tumors

Laura Santana-Viera,[1] Justin P. Dassie,[2] Marta Rosàs-Lapeña,[1] Silvia Garcia-Monclús,[1] Mariona Chicón-Bosch,[1] Marina Pérez-Capó,[1] Lidia del Pozo,[1] Sara Sanchez-Serra,[1] Olga Almacellas-Rabaiget,[1] Susana Maqueda-Marcos,[1] Roser López-Alemany,[1] William H. Thiel,[2] Paloma H. Giangrande,[2] and Oscar M. Tirado[1,3,4]

[1]Sarcoma Research Group, Institut d'Investigació Biomèdica de Bellvitge-IDIBELL, Oncobell, L'Hospitalet de Llobregat, 08908 Barcelona, Spain; [2]Department of Internal Medicine, University of Iowa, Iowa City, Iowa, IA 52242, USA; [3]CIBERONC, Carlos III Institute of Health (ISCIII), Madrid, Spain; [4]Institut Català d'Oncologia (ICO), L'Hospitalet de Llobregat, Barcelona, Spain

The EphA2 receptor tyrosine kinase is overexpressed in most solid tumors and acts as the major driver of tumorigenesis. In this study, we developed a novel approach for targeting the EphA2 receptor using a 2′-fluoro-modified pyrimidine RNA aptamer termed ATOP. We identified the ATOP EphA2 aptamer using a novel bioinformatics strategy that compared aptamers enriched during a protein SELEX using recombinant human EphA2 and a cell-internalization SELEX using EphA2-expressing MDA231 tumor cells. When applied to EphA2-expressing tumor cell lines, the ATOP EphA2 aptamer attenuated tumor cell migration and clonogenicity. In a mouse model of spontaneous metastasis, the ATOP EphA2 aptamer slowed primary tumor growth and significantly reduced the number of lung metastases. The EphA2 ATOP aptamer represents a promising candidate for the development of next-generation targeted therapies that provide safer and more effective treatment of EphA2-overexpressing tumors.

INTRODUCTION

Various solid tumors, such as ovary,[1,2] prostate,[3,4] pancreas,[5] glioblastoma,[6,7] lung,[8] melanoma,[9,10] esophageal,[11] colorectal,[12–14] bone sarcomas,[15,16] and breast,[17–19] are reported to express high levels of the tyrosine kinase receptor EphA2. Furthermore, we and others have demonstrated that overexpression of the EphA2 receptor plays a key role in the aggressiveness and metastatic potential for many of these tumors.[4,19,20]

EphA2 expression in adult epithelial cells is low and is occupied by the ephrin ligand that is expressed on the surface of adjoining cells. The EphA2-ephrin interaction initiates the established EphA2 signaling cascade.[21] The EphA2 receptor transmits signals that negatively regulate epithelial cell growth, inhibit cell migration, and induce EphA2 internalization and degradation.[22] However, malignant cells demonstrate weakened cell-cell contacts, which prevents association of the EphA2 receptor with ephrin and leads to EphA2 receptor upregulation.[23] EphA2 receptors can also signal in the absence of ligand binding[21,24] and alter downstream signaling in a noncanonical way that contributes to the metastatic process by promoting cell migration and invasion.[24,25] Therefore, EphA2 is a critically important therapeutic target. Agents that promote EphA2 activation can be useful for suppressing cancer cell malignancy. Various strategies have been employed to target and modulate EphA2 activation. Monoclonal antibodies have been developed that mimic the actions of ephrin A1[26,27] and target the large extracellular domain of EphA2 that is frequently upregulated by tumor cells.[28] Peptides and antibodies that bind the ephrin-binding pocket have been used to specifically deliver cytotoxins, but their application is limited due to modest binding affinity.[29–31]

Aptamers are short single-stranded nucleic acid oligomers (ssDNA or RNA) that form complex three-dimensional shapes and bind with high affinity and specificity to target molecules.[32] Aptamers possess key advantages; their production does not depend on bacteria, cell cultures, or animals. Unlike antibodies, aptamers can be chemically synthesized to fine-tune their properties for specific applications such as increasing serum stability, improving pharmacokinetics, and delivering small molecules or imaging agents.[33] Despite the Food and Drug Administration having only approved of one aptamer-based drug,[34] the therapeutic potential of aptamers is confirmed by clinical trials, including the NOX-A12 aptamer that inhibits CXCL12 inhibitor and the ApTOLL aptamer that antagonizes

Received 27 March 2023; accepted 4 May 2023;
https://doi.org/10.1016/j.omtn.2023.05.003.

Correspondence: William H. Thiel, Department of Internal Medicine, University of Iowa, Iowa City, Iowa, IA 52242, USA.
E-mail: william-thiel@uiowa.edu
Correspondence: Paloma H. Giangrande, Department of Internal Medicine, University of Iowa, Iowa City, Iowa, IA 52242, USA.
E-mail: pgiangrande@wavelifesci.com
Correspondence: Oscar M. Tirado, Sarcoma Research Group, Institut d'Investigació Biomèdica de Bellvitge-IDIBELL, Oncobell, L'Hospitalet de Llobregat, 08908 Barcelona, Spain.
E-mail: omartinez@idibell.cat

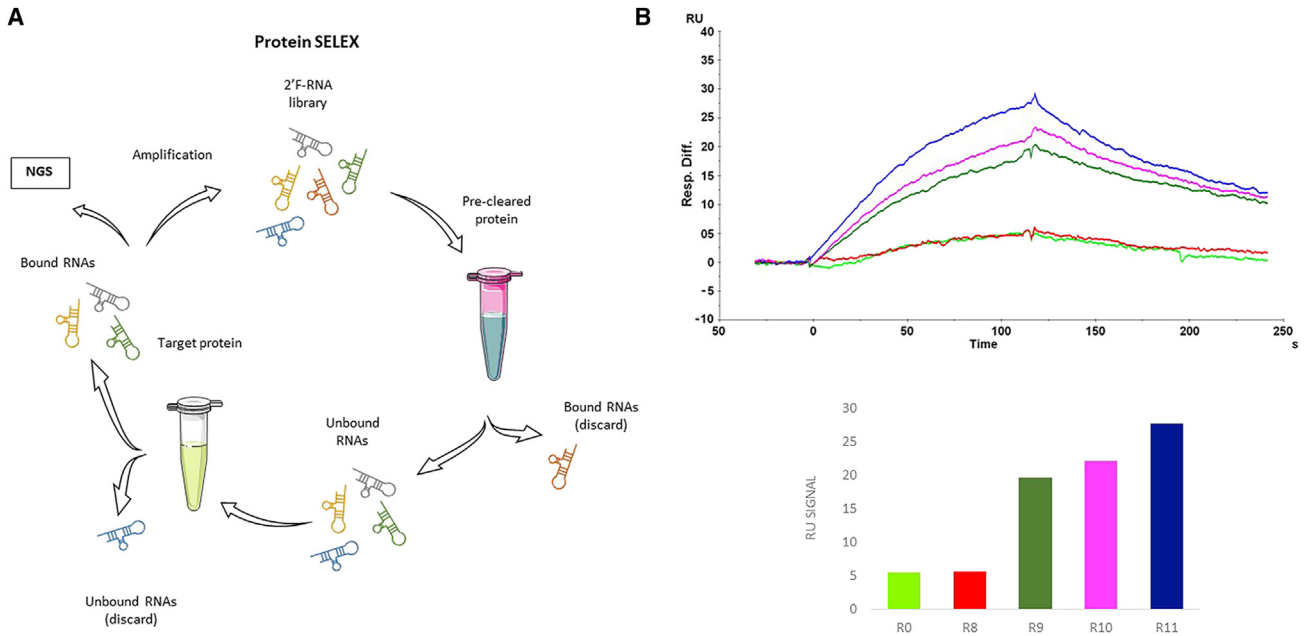

Figure 1. Protein SELEX

(A) Schematic representation of the procedure carried out to individualize rhEpha2 binding aptamers.

(B) Progression of human EphA2 selection was determined via SPR.

Toll-like receptor 4, which demonstrate the safety and efficacy of systemic administration.[35–39]

Aptamers are identified through a simple and economic procedure termed SELEX[40] (systematic evolution of ligands by exponential enrichment). *In vitro* protein-based aptamer selections have the advantage of identifying high-affinity aptamers against a known target protein; however, recombinant purified proteins may not fold into the correct tertiary structures and many of the aptamers identified from protein SELEX may not bind the target protein when expressed by cells.[41] Cell-based aptamer selections have the advantage of identifying aptamers that bind proteins expressed by a target cell population, but the target protein may be unknown or many of the enriched aptamers may have a low affinity for the target protein. In this study, we identified a 2′-fluoro-modified pyrimidine RNA aptamer we termed ATOP (aptamer top of the list) that selectively binds the EphA2 receptor. We identified ATOP using a novel aptamer bioinformatics strategy applying an aptamer clustering algorithm to identify co-enriched aptamers with similar structures from two independent SELEX processes, one using protein SELEX with recombinant EphA2 and a second using cell-internalization SELEX with EphA2-expressing MDA231 cells. We observed that the ATOP EphA2 aptamer exhibits antitumorigenic effects *in vitro* by inhibiting tumor cell migration and clonogenicity. In an *in vivo* orthotopic mouse model of Ewing sarcoma, the ATOP aptamer significantly attenuated tumor growth and significantly reduced metastatic potential. These *in vitro* and *in vivo* data support the clinical potential of the ATOP aptamer as a targeted therapeutic to prevent EphA2-associated tumor growth and metastasis.

RESULTS

Identification of RNA aptamer sequences against rhEphA2 that selectively internalize into EphA2-expressing cells

To identify aptamers that selectively bind to recombinant human EphA2 (rhEphA2), an *in vitro* protein-SELEX procedure (Figure 1A) was performed. To avoid selecting specific tag binding aptamers, a preclear step was introduced before each round of selection (Table S1). Selection was assessed using a surface plasmon resonance (SPR) assay (Figure 1B). Round 8 exhibited significant specificity for rhEphA2 compared with human Her2 (hHer2) used as a negative control (Figure S1). Despite round 9 demonstrating a significant increase in relative binding affinity, the selection was continued for another two rounds to decrease the aptamer library's diversity while simultaneously increasing the overall affinity for the intended target, rhEphA2.

In parallel, a cell-internalization SELEX was conducted to enrich for aptamers that selectively internalize into EphA2-expressing human cells[41] (Figure 2A). The EphA2-expressing MDA231 human breast adenocarcinoma cell line was identified as an ideal cell line due to its high expression of hEphA2 compared with other cell lines (Figure S2B). To ensure specificity of the aptamers, a double counter-selection step was used during the cell-internalization SELEX process. Unbound and surface-bound RNA were discarded after a stringent high-salt wash (0.5M NaCl) allowing for the recovery of internalized aptamers (Table S2). Ten rounds of selection were performed, and

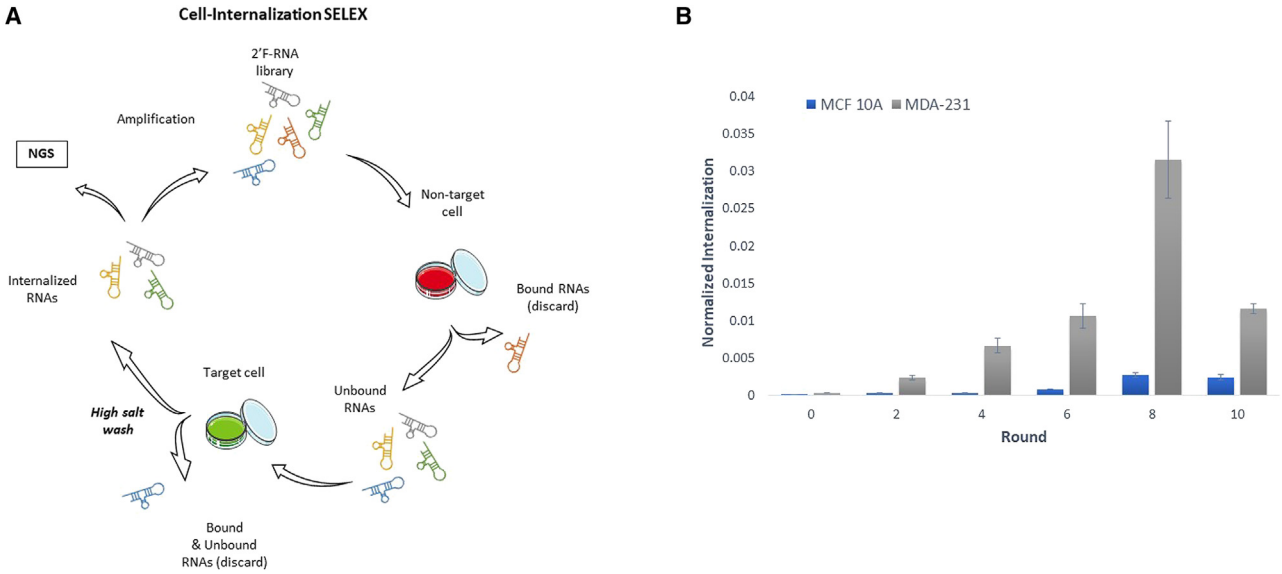

Figure 2. Cell-internalization SELEX

(A) Schematic representation of the procedure carried out to identify aptamers that specifically internalize into EphA2-expressing cells.

(B) Progression of the selection was determined via qRT-PCR adding an internal reference control RNA for normalization. Error bars depict ±SD (n = 3).

cell-specific internalization of each selection round was assessed by quantitative reverse-transcription polymerase chain reaction (qRT-PCR) (Figure 2B).

The starting aptamer libraries and all selection rounds from both the cell-internalization SELEX and protein SELEX were prepared for next-generation sequencing (NGS) on the Illumina platform. NGS data from both selections were analyzed to generate a non-redundant database of all unique aptamers with normalized read counts[42] from each selection round. From this dataset, aptamer sequences were evaluated and filtered for a continuous positive log2 fold change (log2FC $\geq$ 1) enrichment across selection rounds to identify potential candidates. From this analysis, 753 aptamer candidates were identified from the cell-internalization SELEX and 857 aptamer candidates were identified from the protein SELEX that exhibited continuous positive log2FC enrichment. Next, an unpublished updated version of an aptamer clustering algorithm[43] was applied to identify convergent structural motifs between the two selections. Our working hypothesis was that a subset of aptamers from the cell-internalization SELEX could be identified that share a common sequence/structural motif with aptamers enriched during the protein SELEX for the hEphA2 receptor. These aptamers would be capable of targeting the hEphA2 receptor expressed by cells. The clustering algorithm predicts the most likely secondary structure using RNAfold[44] (Vienna Package 2.0) of each aptamer and then calculates the tree distance[45] between pairs of predicted structures using RNAdistance (Vienna Package 2.0). The clustering algorithm generates networks of aptamers within a set maximum tree distance that can be visualized using Cytoscape.[46] The clustering algorithm was run with increasing thresholds of tree distance until aptamers from the two different selections exhibited inter-connections (Figure 3A). The clustering algorithm can also examine sequence relatedness; however, structural clustering was given priority due to the different lengths of the starting libraries (N20 vs. N30). The aptamer from the protein SELEX with the greatest number of connections with the cell-internalization SELEX aptamer was identified (Figure 3B) and used to create a sub-network of that aptamer and all directly connected aptamers (Figure 3C). The aptamer structures from within this sub-network were visually compared with obtain a common sequence/structure motif (Figure 3D), termed ATOP.

Specificity of the selected aptamer toward the target protein

To validate the specificity and affinity of ATOP for human EphA2, the dissociation constant (K_D) of ATOP for hrEphA2 was determined by SPR (BIAcore). Human recombinant EphA2 was immobilized and the binding kinetics with different concentrations of ATOP was measured (Figure 4A). The apparent K_D of ATOP for hrEphA2 was observed to be within the picomolar range. Next, we evaluated the ability of the aptamer to bind to the EphA2 receptor in the context of a Ewing sarcoma cell line that naturally expresses high levels of EphA2 on the cell surface, such as A673 (ES) (Figure S2A). The K_D was calculated using 5′-end cyanine 5 (Cy5)-labeled aptamers and flow cytometry. The binding data, obtained as mean fluorescent intensity (MFI), were fitted after subtracting data attained from a non-related scramble sequence (SCR) used as a normalization control. The K_D indicated that ATOP had high affinity for A673 cells, with a value in the nanomolar range (Figure 4B). To further confirm specificity for EphA2-expressing tumor cells, a pull-down assay was performed with biotinylated ATOP and SCR control aptamer using cell extracts from A673 cells. The ATOP aptamer was able to pull-down endogenous EphA2 with high specificity, whereas only low non-specific binding was detected with the SCR control

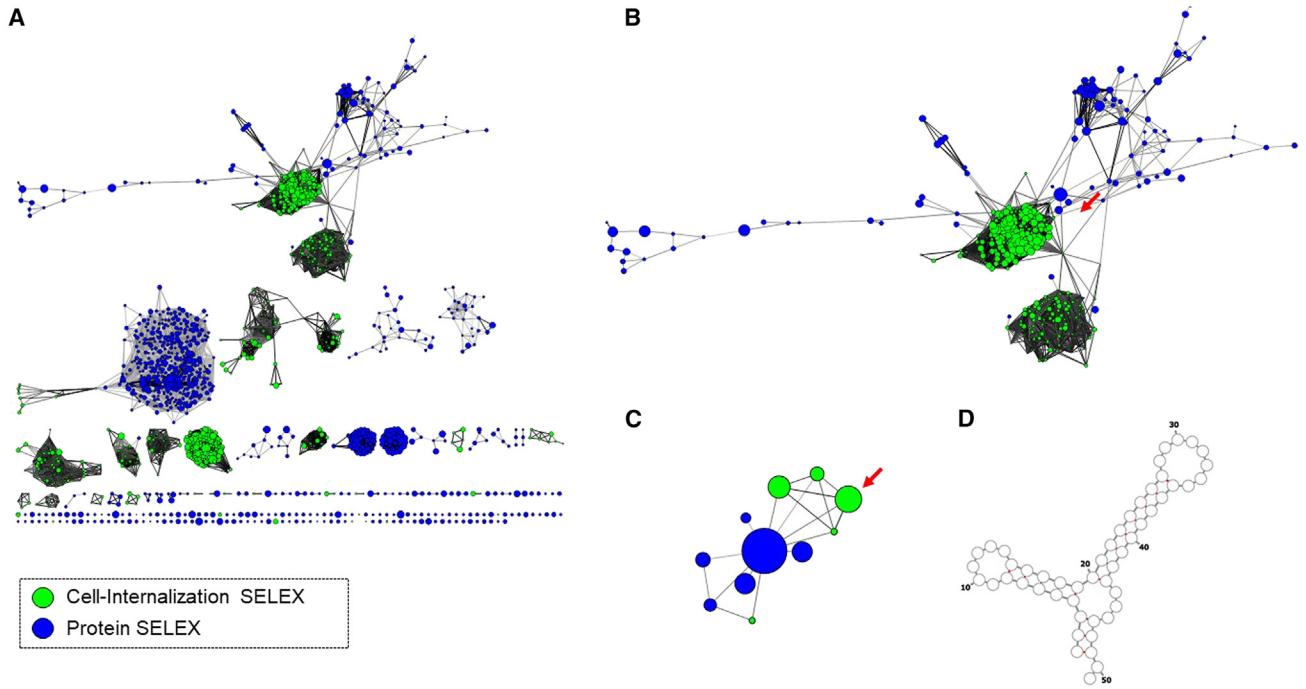

Figure 3. Networks of cell-internalization SELEX aptamers and protein SELEX aptamers related by predicted secondary structure

(A) Interconnected aptamers (nodes) with structural similarity between cell-internalization SELEX (green nodes) and protein SELEX (blue nodes).

(B) One network included nodes from both SELEX processes. Red arrow highlights the node from protein SELEX presenting most inter-connections with aptamers from cell-internalization SELEX.

(C) Isolation of the protein SELEX aptamer nodes and all directly connected nodes from both the protein and cell-internalization SELEX. Red arrow indicates the cell-internalization SELEX aptamer with the largest number of reads and greatest log2FC enrichment identified as ATOP.

(D) ATOP aptamer secondary structure predicted by using RNA Structure version 6.3.

aptamer (Figure 4C). Together, these data confirmed the success of the parallel SELEX strategy using protein SELEX and cell-internalization SELEX for identifying aptamers that bind rhEphA2 with high affinity.

Aptamer serum stability

An important characteristic of aptamers for their applicability in the biomedical field is represented by their stability, as RNA is very sensitive to nuclease degradation. ATOP contains 2′F-Py modifications that confer resistance to nuclease degradation. We examined the stability of the ATOP aptamer incubated in human serum (50%) over time. We observed that the ATOP aptamer is stable for 8 h in human serum followed by gradual degradation (Figure 5A). The approximate human serum half-life as determined by band intensity quantification (Figure 5B) was 48 h.

Internalization capability and functional aspects of the aptamer

To serve as a therapeutic, the ATOP aptamer must be able to internalize into EphA2-expressing cells in a receptor-dependent manner, mimicking the antitumorigenic effect that EphA2's natural ligand provokes. The internalization potential of ATOP was evaluated with A673 cells and RH4 cells, an alveolar rhabdomyosarcoma (ARMS) cell line, that both express high levels of EphA2 (Figure S1A). The ATOP aptamer or the SCR control aptamer were incubated on cells for 1 h and the internalized aptamer RNA recovered after a stringent high-salt wash (0.5M NaCl) was assessed by qRT-PCR. As expected, the ATOP aptamer internalized into EphA2 overexpressing cells significantly better than the SCR control aptamer in both the A673 and RH4 cells (Figure 6A). Moreover, ATOP internalization was performed in MDA-MB-231 cells for 30 min to corroborate that the mechanism of internalization was receptor specific. Interestingly, at shorter times, only ATOP could be detected inside the cells (Figure S3). To confirm these results, we treated the A673 and RH4 cells with fluorescently labeled (Cy5) ATOP and SCR aptamer and assessed internalization by flow cytometry following the same stringent high-salt wash described above. We observed the same trend with significantly more internalized Cy5 ATOP associated with the A673 and RH4 cells compared with the Cy5 SCR control aptamer (Figure 6B). Next, we compared ATOP internalization with the A673 cells that highly expressed EphA2 against RH28 cells, another ARMS cell line that expresses significantly lower EphA2. As anticipated, the ATOP aptamer internalized preferentially to A673 cells over the RH28 cells (Figure 6C). To visualize the aptamer localization within the cell we performed fluorescence microscopy on the A673 cell line treated with Cy5 ATOP aptamer and co-stained for the EphA2 receptor (Figure 6D and Figure S4). We observed that the majority of the ATOP aptamer resides within the cytoplasm of the A673 cells, suggesting ATOP aptamer internalization.

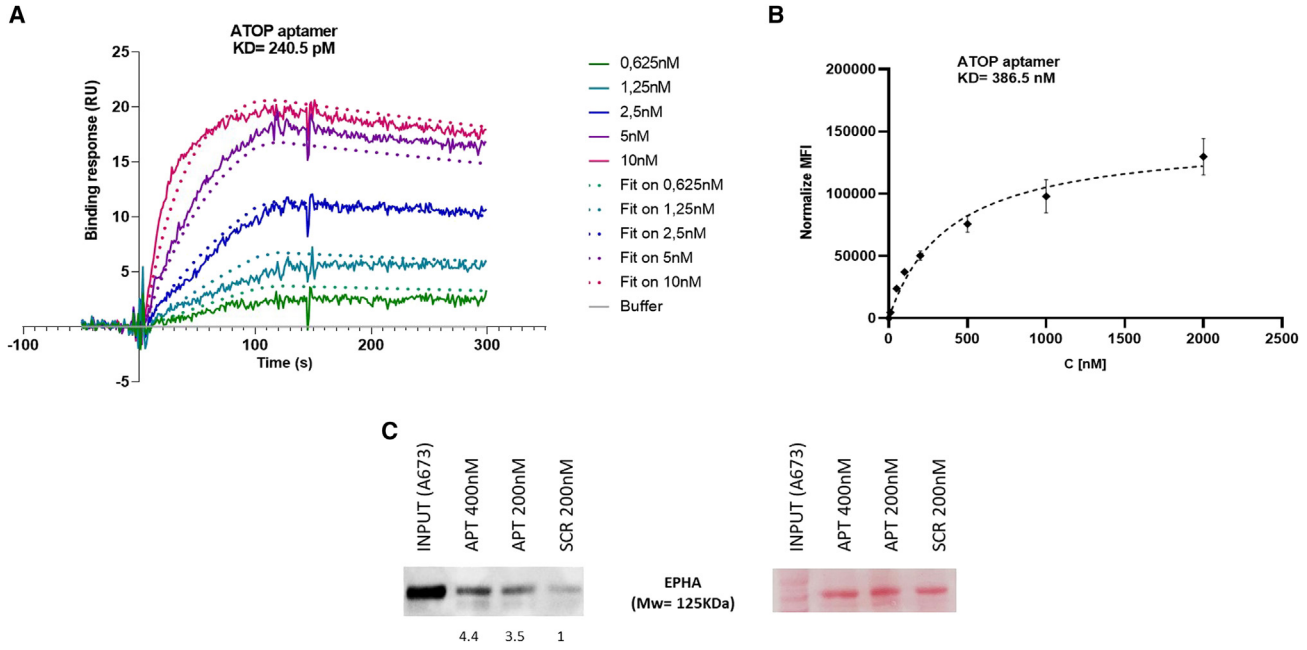

Figure 4. Binding specificity of the selected aptamer

(A) Binding curve of ATOP toward recombinant human EphA2 evaluated by SPR. A value for the dissociation constant K_D of 240.5 pM was calculated using BIAevaluation 4.1 software.

(B) Binding curve of ATOP toward EphA2-expressing A673 cell line evaluated by FACS. The binding data, obtained as MFI, were fitted after being subtracted from the SCR. A value for the dissociation constant K_D of 386.5 nM was calculated with GraphPad Prism 9. Error bars depict ±SD (n = 3).

(C) Aptamer-mediated pull-down. A673 cell lysates (500 ng) were incubated with 200 or 400 nM of APT or control aptamer (SCR), purified on streptavidin beads and immunoblotted with anti-EphA2 antibody. Fifty micrograms of total cell extract (input) was loaded as reference. Bands intensities were calculated using Fiji software and fold change with respect to the SCR control sequence is expressed below the right image. A ponceau of the membrane was performed for loading control (right image).

We next examined the functional effect of ATOP aptamer internalization on the clonogenicity and migration capability of several tumor cell lines from different tumor types, including ES, ARMS, or triple-negative breast cancer (TNBC) that overexpress EphA2 membrane receptor (Figure S2A). To assess clonogenicity, cells were seeded at a low density and treated with either ATOP aptamer or SCR control aptamer starting at 24 h. Cells were treated with aptamer every 3 days until the formation of clones was observed with the control cells (approximately 15 days). The ATOP aptamer attenuated clonogenicity potential of the tumor cells at concentrations as low as 100 nM (Figures 7A and 7B). To assess migration capability, cells were pre-treated with 250 nM of the ATOP aptamer or the SCR control aptamer for 6 h before transwell migration assay. The ATOP aptamer reduced the migratory capacity of tested cells with no effect on the migratory capacity of the cells treated with the SCR control aptamer (Figures 7C and 7D).

These results confirm that ATOP is a promising candidate for targeting EphA2 receptor while exerting a therapeutic effect. Given the reported role of the EphA2 receptor in cancer, the effect induced by ATOP treatment is likely due to its capacity to internalize in a receptor-specific manner, thus promoting the receptor degradation that diminishes the tumorigenicity capacity of the tested cells (Figure S5).

In vivo experiments

For the analysis of aptamer biodistribution, a fluorescently labeled ATOP aptamer and SCR control aptamer bearing a cyanine7 (Cy7) moiety were used. A single dose of Cy7-ATOP or Cy7-SCR, at a concentration of 1.6 mg/kg was injected intravenously (i.v.) via tail vein of the mice bearing a tumor (A673 cells) of approximately 800 mm^3. Fluorescence of tissues from treated mice was measured at different time points. At 30 min post-injection, both aptamers were detected within the abdomens of treated mice. Fluorescence peaked at 1 h and decreased quickly until 72 h, when a small signal could be detected (Figures 8A and 8C). Fluorescence in the tumor of Cy7-ATOP aptamer-treated mice could be detected 8 h post-injection, with the signal increasing until 72 h. In contrast, the Cy7-SCR control aptamer was not detected in the tumor at any time point. Following euthanasia at 72 h, fluorescence was detectable in the liver and kidneys for both aptamers. Only fluorescence in the tumor was detected with Cy7-ATOP, while Cy7-SCr yielded no signal in the tumor (Figure 8B). These results support that the Cy7-ATOP aptamer accumulated specifically in the primary tumor comprised of EphA2-expressing A673 cells, while the control aptamer, Cy7-SCR, did not.

Following confirmation that the ATOP aptamer reached the sarcoma tumor, inhibition of tumor growth or metastasis formation was evaluated using a previously described metastatic assay.[47] With this

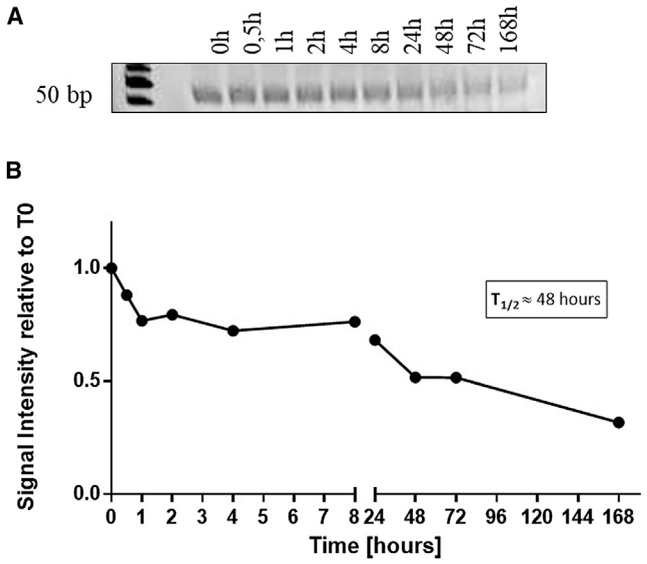

Figure 5. Aptamer serum stability was measured in 50% human serum at the indicated times

(A) At each time point, RNA-serum samples were collected and evaluated by electrophoresis in a 15% denaturing polyacrylamide gel. Gel was stained with ethidium bromide and visualized using a Gel Doc EZ Imager. (B) Bands were quantified using ImageJ.

model, luciferin-labeled A637 Ewing sarcoma tumor cells are injected into the gastrocnemius muscle in athymic immunodeficient mice. Once the tumor volume exceeds 800 mm^3 (~15–20 days after inoculation) the gastrocnemius muscles are surgically resected, and the occurrence of lung metastasis is observed by *in vivo* luciferin reading of the whole mice or *ex vivo* luciferin detection of the lung. Mice were treated with the ATOP aptamer or SCR control aptamer at a dose of 1.6 mg/kg via i.v. tail vein injection every third day, from day 1 through day 22. Tumor volumes were smaller in ATOP aptamer-treated mice compared with SCR aptamer-treated mice. Furthermore, time to gastrocnemius muscle surgery was significantly extended by the ATOP aptamer (Figure 8D). Following gastrocnemius muscle resection, the incidence in lung metastasis was reduced to 22% with the ATOP aptamer-treated mice compared with SCR aptamer-treated mice (Figure 8E). Thus, ATOP aptamer, selected for EphA2 specificity, effectively inhibited primary tumor growth, delayed time of surgery, and reduced lung metastasis in athymic mice.

DISCUSSION

In this study we identified an EphA2 2′-fluoro-modified pyrimidine RNA aptamer ATOP that, in an *in vivo* mouse model of Ewing sarcoma metastasis, slowed primary tumor growth and reduced the number of lung metastases. The ATOP EphA2 aptamer was identified using an aptamer clustering algorithm to identify a common sequence-structure motif between two parallel selections: protein SELEX[48] using hEphA2 and cell-internalization SELEX[49] using MDA231 cells that express EphA2. This strategy leverages the strengths associated with each SELEX process to identify aptamers that recognize a target protein in its endogenous conformation with high affinity and offers an alternative to Toggle SELEX, Hybrid SELEX,[50] and Ligand Guided Selection SELEX.[51] Conducting the two SELEX strategies independently of each other and then bioinformatically comparing them using the clustering algorithm has two distinct advantages over integrated SELEX strategies such as Toggle SELEX. First, the rigor of a common sequence-structure motif containing aptamers being enriched for the same target across two disparate SELEX strategies. Second, conducting two independent SELEX methods does not require alternating SELEX methods, which may impart an unintended bias. For example, should a toggle SELEX start with the protein SELEX first or the cell-internalization SELEX? However, one distinct disadvantage of our method is that two independent SELEX processes requires more effort than a single Toggle SELEX.

The ATOP EphA2 aptamer is distinguished from other aptamers that have been recently described as potential EphA2 targeting moieties.[52,53] The latter studies used an unbiased cell-based SELEX process that required identification of the target protein after the aptamer selection using biochemical methods (e.g., protein pull-down followed by mass spectrometry). Interestingly, the affinity for these EphA2 aptamers, A40s and EA-3, does not reach the affinity reached by the ATOP aptamer. An ELONA assay was used to determine the K_D of the A40s aptamer for recombinant EphA2 (K_D = 0.76 ± 0.2641 nM). The EA-3 aptamer K_D for recombinant EphA2 was not reported. Potentially, the higher affinity of the ATOP aptamer compared with these other EphA2 aptamers for EphA2 may be due to how we identified ATOP using data from both a protein-based SELEX and cell-internalization SELEX.

In recent years, accumulated evidence has suggested that EphA2 and its ligands influence human cancer initiation, tumor growth, and metastasis. EphA2 overexpression has been shown both at the mRNA and protein levels in established cell lines and human tumor tissue specimens. Data from different studies suggest that the receptor is overexpressed in 61% of glioblastoma multiforme patient tumors,[54] 76% of ovarian cancers,[1] 85% of prostate adenocarcinomas,[55] and 95% of pancreatic carcinomas.[56] In contrast, EphA2 protein expression in normal tissue is typically low, except for tissues that contain a high proportion of dividing epithelial cells, such as the brain, colon, urinary bladder, uterus, testis, and prostate; nevertheless, its expression is still lower than in tumor samples.[57] Based on these observations, EphA2 is a promising therapeutic target for cancer treatment. Several targeting regimens, including antibodies, peptides, small-molecule inhibitors, and ADC, have shown significant antitumor activities alone or in combination with other therapies in EphA2-positive cancer models.[21] Therefore, ATOP might represent a great opportunity to target EphA2 to treat these tumors. Nevertheless, further studies must confirm the ATOP aptamer specificity for EphA2 including evaluating the affinity for other members of the ephrin family of receptors. The internalization capacity of the ATOP aptamer should be further evaluated for EphA2-expressing cells and confirmation of the antitumorigenic response we observed with the mouse model of Ewing sarcoma

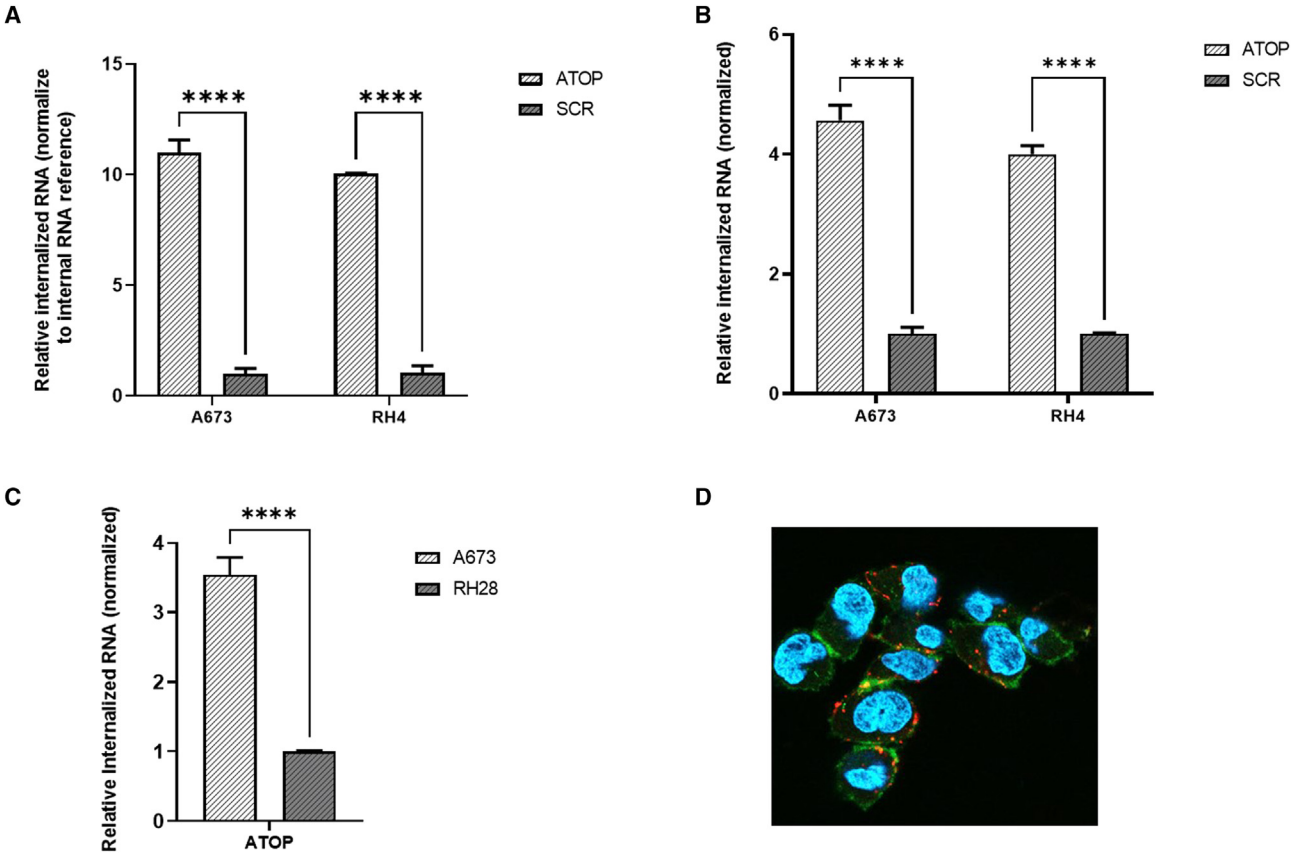

Figure 6. Internalization of the aptamer into cells

(A) Aptamer (ATOP and SCR) internalization into RH4 and A673 was evaluated by qRT-PCR and normalized to an internal RNA reference control for PCR. Efficiency of internalization shown is relative to the SCR sequence.

(B) Internalization of fluorescent labeled aptamers (ATOP and SCR) into RH4 and A673 was measured by flow cytometry (MFI) and normalized against the SCR sequence.

(C) Discrimination of ATOP internalization between Epha2^{+} (A673) and EphA2^{-} (RH28) cells was evaluated by flow cytometry (MFI) and normalized against the SCR sequence.

(D) Confirmation of ATOP internalization on A673 was done using confocal laser scanning microscopy. DAPI (cyan), EphA2 (green), and ATOP-Cy5 (red). Data are presented as means ± SD. Statistical significance was achieved by Student's t test from at least three different experiments: ****$p \leq 0.0001$.

metastasis. It has been widely described that EphA2 activation upon ligand binding decreases the oncogenic signaling within tumor cells and causes its rapid degradation upon internalization.[24,58] This observation is in concordance with our results showing that the ATOP aptamer can reduce chemotactic cell migration and colony formation *in vitro* on several EphA2-positive cell lines. Furthermore, *in vivo*, we have evidence of ATOP aptamer accumulation within tumors *in vivo* that is associated with a reduction in tumor development and lung dissemination.

Altogether, the potency and selectivity of ATOP suggests an opportunity to develop a highly potent and safe therapeutic strategy for the treatment of cancers that overexpress EphA2. In fact, the internalization capabilities of the ATOP aptamer suggest that it may be used as a delivery vehicle based on existing aptamer conjugate technology with small interfering RNAs (siRNAs). RNA interference therapeutics represent a fundamentally new avenues to treat human disease by addressing targets that are otherwise "undruggable."[59] To achieve efficient therapeutic posttranscriptional gene-silencing, siRNAs must be selectively delivered to diseased cells and tissues. This specific delivery to disease cells is one of the main hurdles for translating siRNAs for clinical use. An important breakthrough for targeted siRNA delivery was the use of GalNAc, a carbohydrate moiety that binds with high affinity to the highly liver-expressed asialoglycoprotein receptor 1 (ASGR1, ASPGR) and facilitates the uptake of antisense oligonucleotides and siRNAs into hepatocytes by endocytosis.[60] However, for targeting other tissues than the liver, novel moieties must be identified, and aptamers are a viable alternative. From this perspective, aptamer-linked siRNA chimeras are a promising tool that has been widely explored in the last decade.[61] Likewise, drug conjugates comprising a tumor-homing carrier tethered to a cytotoxic agent via a linker that are designed to deliver an ultra-toxic payload directly to the target cancer cells is another promising use for ATOP. Drug conjugates using antibodies as carriers are being developed worldwide.[62] However, these antibody-drug conjugates (ADCs) have encountered several limitations for their use

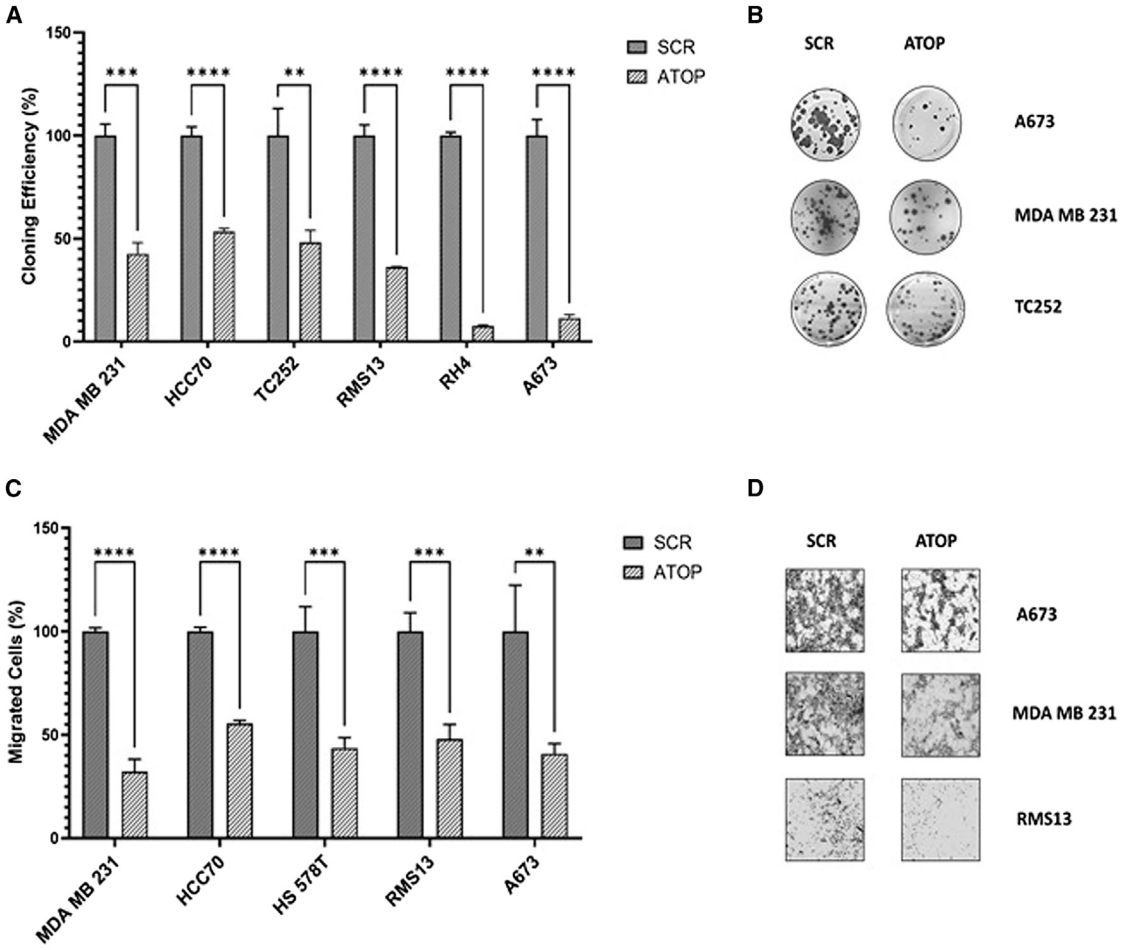

Figure 7. Functional effect of ATOP on EphA2⁺ tumor cell lines

(A) Quantification of the colony formation assay. Cells were treated with 100 nM of ATOP or SCR every 72 h for 15 days and their capacity to form clones was evaluated.

(B) Representative images of cells stained with crystal violet.

(C and D) Quantification of the migration assay in Boyden chambers. Cells were treated with 250 nM of ATOP or SCRA for 6 h before being subjected to migrate for 24 h. Representative images of stained cells that migrated to the other side of the membrane are shown in (D). Data are presented as means ± SD. Statistical significance was achieved by Student's t test from at least three different experiments: $^{**}p \leq 0.01$, $^{***}p \leq 0.001$, $^{****}p \leq 0.0001$.

in targeted delivery. Mainly, they are protein based, and thus are difficult to manufacture, especially in large scale, as the risk of batch-to-batch variation is high. Secondly, if used long term, there is the potential of stimulating an anti-drug antibody response to the drug, inactivating the drug. Therefore, use of ADC is a key milestone. Other delivery systems must be developed to overcome the aforementioned limitations and, indeed, other classes of drug conjugates are emerging. A potential alternative may be cell-penetrating peptides (CPPs), a diverse class of tailored peptides with well-developed cell-permeability characteristics. However, CPPs are not cell-type specific, hampering their clinical use.[63]

In contrast, aptamers are produced by chemical synthesis, a more reliable process of large-scale production. In addition, aptamers are much less immune-stimulating. Further characterization and understanding of the long-term effects of their use is needed, as aptamers have not been on the market for long. Finally, aptamers have a smaller molecular weight (~20,000 vs. ~150,000 Da for mAbs) and easily penetrate tissues, including tumors, when used for therapeutic purposes.[38] Moreover, their smaller size may help minimize off-targeted effects, as the drug that does not reach the target will be quickly secreted. The superior performance of aptamers over antibodies in tumor penetration has been addressed by Xiang et al.[64] Yet, despite the fact that aptamers can be chemically modified to decrease their susceptibility to degradation by nucleases and increase their circulating half-lives, antibodies still present a better stability in circulation and a lower degradation rate.

Further studies are needed to optimize aptamers before they become a powerful tool for delivering either RNA therapeutic molecules or

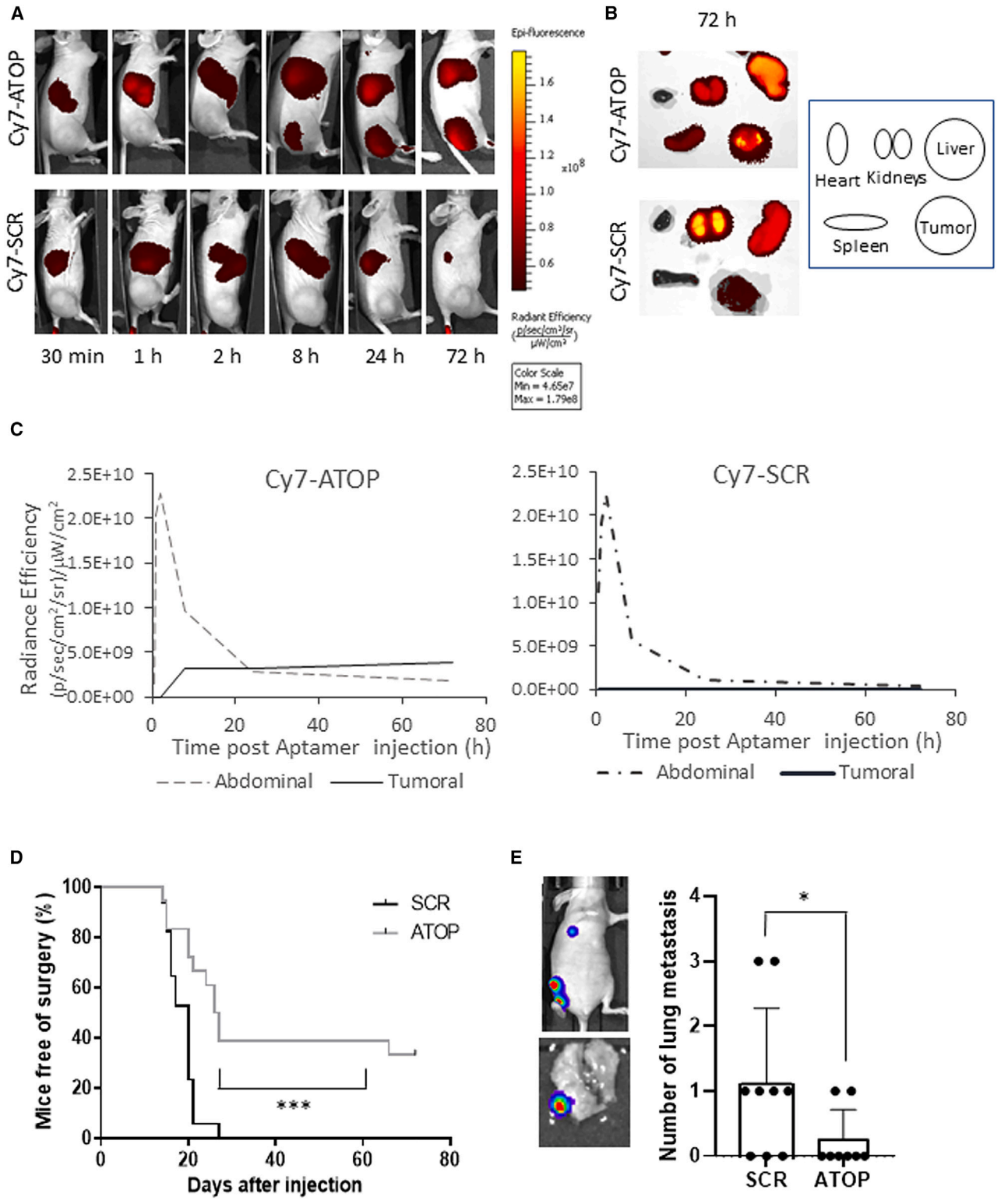

(legend on next page)

conjugated standard of care for a more specific and effective treatment. Nevertheless, the therapeutic potential of ATOP alone, combined with the amount of information interlacing EphA2 with cancer progression, warrants success for this RNA aptamer as an antitumoral targeted oligonucleotide therapy.

MATERIALS AND METHODS

Cell lines

Cell lines were either donated or acquired: A673 and TC252 (ES) were gifted from Dr. Heinrich Kovar (St. Anna Children's Cancer Research Institute, Vienna, Austria); RH4 (ARMS) was gifted from Dr. Peter Houghton (The Research Institute at Nationwide Children's Hospital, Columbus, OH); RH28 and RMS13 (ARMS) were gifted from Dr. Beat Schäfer (Department of Oncology and Children's Research Center, University Children's Hospital, Zurich, Switzerland); MDA-MB-231, HS-578T, and HCC70 (TNBC) were purchased from the German Collection of Microorganisms and Cell Cultures (DSMZ, Braunschweig, Germany). HEK293, hTERT, and MDA-MB-231, used for the cell-internalization SELEX, were acquired from the American Type Culture Collection (ATCC, Manassas, VA).

Cells were cultured in RMPI 1640-GlutaMAX medium supplemented with 10% (v/v) heat-inactivated fetal bovine serum (FBS) and 1% (v/v) penicillin/streptomycin and were incubated at 37°C in a humidified atmosphere of 5% CO_2 in air. Unless otherwise specified, cell culture reagents were purchased from Gibco (Thermo Fisher Scientific, Waltham, MA). Exponentially growing cells within two sequential passages were used for all experiments. Cells were routinely tested for mycoplasma.

RNA library and primers

For the SELEX procedure, a 2′-fluoro-pyrimidine (2′-F-Py)-modified RNA library with a variable region of 30 nucleotides (nt) for the *in vitro* SELEX and 20 nt for the cell-internalization SELEX, and two fixed regions of 16 nt for the amplification reaction, was generated by *in vitro* transcription using a mutant Y639F T7 RNA polymerase and chemically synthesized DNA templates (IDT). The *in vitro* transcription reactions for the library and all subsequent rounds of SELEX were supplemented with 2′-fluoro-modified CTP and UTP (TriLink BioTechnologies, San Diego, CA) to generate RNAs that were nuclease resistant.

The forward selection primer sequence was: 5'-TAATACGACTCAC TATAGGGAGGACGATGCGG-3'; and the reverse selection primer was: 5′-TCGGGCGAGTCGTCTG-3′. The forward primer contained a T7 promoter sequence for the *in vitro* transcription.

In vitro protein SELEX

Iterative rounds of selection were carried out by modifying the previously described SELEX protocol.[40,65]

Recombinant human EphA2 (R&D Systems, Minneapolis, MN, cat. no. 3035-A2) was used as the target protein in the selection step, whereas recombinant human glyoxalase (R&D Systems, cat. no. 4959-GL) was used as the pre-cleared protein in the counter-selection step. Recombinant human Her2 (R&D Systems, cat. no. 10126-ER) was used for specificity checking. All proteins contained a C-terminal 6-histidine tag to allow binding with the cobalt-conjugated magnetic beads (Dynabeads Talon, cat. no. 101.01D, Invitrogen, Waltham, MA) that were used to separate aptamer-His-tagged protein complexes.

Before each cycle, cobalt-conjugated magnetic beads previously washed with binding buffer (BB; 20 mM HEPES [pH 7.4], 150 mM NaCl, and 2 mM $CaCl_2$) were incubated in the presence of target or pre-clear protein at 37°C for 20 min with occasional agitation. Each round of SELEX was started with a counter-selection step to avoid selecting for aptamers that non-specifically recognize the target protein: 2 nmol of 2′-F-Py-RNA was first incubated with the preclear protein (recombinant human glyoxalase) immobilized on magnetic beads at 37°C for 30 min. Supernatant from this incubation was then transferred to target protein immobilized on magnetic beads and again incubated at 37°C for 30 min for the selection step. Unbound RNAs were removed by washing several times with the binding buffer, whereas the bound sequences were recovered by total RNA extraction using the TRIzol Reagent (Invitrogen). Extracted RNAs were reverse transcribed, PCR-amplified, and the DNA template was *in vitro* transcribed to generate the 2′-F-Py-RNA that was utilized in the subsequent round of selection. During the selection process, selective pressure was enhanced progressively by increasing the numbers and times of washings and by decreasing the concentration of the target protein used (Table S1).

Cell-internalization SELEX

The selection is a modification of the previously described cell-internalization SELEX.[49,66]

Several cell lines expressing low levels of EphA2 (HEK293, hTERT, and MCF10A) were used in the counter-selection step to maximize

Figure 8. *In vivo* assay

Biodistribution of Cy7-ATOP and Cy7-SCR in an orthotopic model of sarcoma tumors.

(A) Real-time biodistribution of Cy7-ATOP and Cy7-SCR in an orthotopic model of sarcoma tumors at different time points. Representative images of n = 3 are shown. Mice were imaged at different time points using IVIS on lateral view.

(B) *Ex vivo* imaging of major organs and tumors after euthanasia, 72 h after i.v. aptamer injection.

(C) Quantification of abdominal and tumoral radiance efficiency on aptamer-treated mice.

(D) Mice free of surgery (Kaplan-Meier plots) of aptamers treatment on tumor-bearing mice (n = 20). ***$p < 0.0001$ by Mantel-Cox test.

(E) Incidence of lung metastasis in aptamer-treated mice (n = 10). *$p \leq 0.01$ by Student's t test.

the negative selection process and augment the potential to identify an aptamer specific to the EphA2 receptor in the context of the cell membrane. MDA-MB-231 (EphA2$^+$) was used as the target cell line for the selection step, as it highly overexpresses the receptor (Figure S1B). All cell incubations were carried out at 37°C with 5% CO_2.

In each round the prepared random 2′-F-Py-RNA pool was diluted in DPBS+/+ buffer (Gibco) supplemented with 100 mg/mL yeast tRNA (Invitrogen). Two counter-selection steps using two different EphA2-negative cell lines were performed before the selection step (Table S2). This was done to avoid selecting RNA sequences that internalize through other RTKs. The supernatant (containing RNA aptamers that do not internalize into the non-target cells) was then transferred to target cells. To remove unbound and surface-bound aptamers, target cells were washed with ice-cold DPBS adjusted to 0.5M NaCl (high-salt wash) for 5 min, ensuring that the recovered RNA corresponded to the fraction that was internalized. The extracted RNA was then reverse transcribed into DNA, PCR amplified, and *in vitro* transcribed to RNA, then subjected to the next cycle. To increase the stringency of the selection and promote a faster enrichment of the 2′-F-Py-RNA pool, internalization times and RNA concentrations were reduced, while the number of washes was increased.

NGS and aptamer bioinformatics analysis

Aptamer selection round dsDNA was prepared for NGS[42,49] by PCR using primers that contained Illumina adapter sequence and a unique barcode for each selection round. Amplicons were agarose gel purified, concentration determined by Qubit, pooled, and quality assessed by Agilent Bioanalyzer. Pooled amplicons were sequenced using the Illumina HiSeq platform. Reads were filtered for quality and data were processed to identify the variable region of the sequenced aptamers and compiled into a single database.[42] Aptamers were analyzed for structure similarity using an unpublished updated version of an aptamer clustering algorithm (https://github.com/uicts/aptamer) developed by W.H.T.[43]

SPR measurements

(1) For monitoring of the *in vitro* selection, SPR measurements were performed with a BIAcore 3000 (GE Healthcare Life Sciences, Boston, MA) in BB (20 mM HEPES [pH 7.4], 150 mM NaCl, and 2 mM $CaCl_2$). The immobilization of histidine-tagged human EphA2 (56.9 kDa, R&D Systems, no. 3035-A2) on a CM5 sensor chip was performed under standard conditions recommended by the manufacturer (GE BIAcore) and protocols described previously.[67,68] After immobilizing human EphA2 onto CM5 chips (Cytiva, Marlborough, MA), 2′-F-Py-RNA from select rounds of selection were subsequently passed over the chip. The flow rate was set at 5 μL/min, and the EphA2 aptamers were injected at a concentration of 10 μM over the sensor chip for 5 min at 37°C (association and dissociation time). After each run, the surface was regenerated with 50 mM aqueous NaOH for 5 s at 15 μL/min. To correct for refractive index changes and instrument noise, the response of the control surface data was subtracted from the responses obtained from the reaction surface using GE BIAcore.

(2) For the determination of the dissociation constant of the selected ATOP aptamer, SPR experiments were carried out at Aptarion Biotech AG (Berlin, Germany). A BIAcore 2000 instrument (GE Healthcare Life Sciences) equipped with a C1 sensor chip (Cytiva) was used. The recombinant human EphA2 receptor (56.9 kDa, R&D Systems, no. 3035-A2) was immobilized using amine-coupling chemistry. In brief, after the chip was equilibrated with 10 mM HEPES and 150 mM NaCl (pH 7.4), the surfaces of the flow cells were activated for 10 min with a 1:1 mixture of 0.1 M NHS (N-hydroxysuccinimide) and 0.4 M EDC (3-(N,N-dimethylamino) propyl-N-ethylcarbodiimide) at a flow rate of 10 μL/min and at a temperature of 37°C. The EphA2 receptor at a concentration of 40–90 nM in 10 mM sodium acetate (pH 4.0) was immobilized at a density of ∼200 RU. On a reference flow cell, 600 nM bovine serum albumin (66.5 kDa) in 10 mM sodium acetate (pH 5.0), was immobilized at a comparable density. Both flow cells were blocked with a 7-min injection of 1 M ethanolamine (pH 8.0). To collect kinetic binding data, concentrations series of the aptamers in 20 mM HEPES, 150 mM NaCl, and 2 mM $CaCl_2$ (pH 7.4) supplemented with 0.01% Tween 20, were injected over the two flow cells at a flow rate of 30 μL/min and at a temperature of 37°C. The complex was allowed to associate and dissociate for 120 and 150 s, respectively. The surfaces were regenerated with 1 M NaCl for 30 s. After subtracting the response of the aptamers on the reference surface and the response of the buffer itself from the binding response (double referencing), the resulting binding curves were fitted to a Langmuir 1:1 stoichiometric binding model to determine the kinetic constants. Data analysis was done using the global data analysis option available within BIAevaluation 4.1 software.

Serum stability

Aptamer was incubated at 4 μM in 50% type AB human serum (Euroclone, Milano, Italy) for 1 h to 7 days. At each time point, 16 μL (64 pmol RNA) was withdrawn and incubated for 1 h at 37°C with 2 μL of proteinase K solution (600 mAU/mL) (QIAGEN, Hilden, Germany) to remove serum proteins that may interfere with electrophoretic migration. Following proteinase K treatment, 18 μL denaturing RNA dye (Invitrogen) was added to the samples that were then stored at −80°C. All time point samples were separated by electrophoresis into 15% denaturing polyacrylamide gel (7 M urea). The gel was stained with ethidium bromide and visualized by UV exposure.

Cell-binding and cell-internalization assays

(1) The qRT-PCR method was used. The indicated cells were plated in a six-well plate at a density of 3×10^5 per well. Twenty-four hours after plating, cells were washed with serum-free medium and incubated with 100 μg/mL yeast tRNA in serum-free medium at 37°C for 15 min (blocking

step). Aptamers were then added to the cells at a concentration of 200 nM and incubated for 1 h at 37°C, gently swirling every 30 min. A scramble RNA sequence (SCR) was used as a negative control. Unbound RNA aptamers were discarded, and cells were washed first with cold PBS, followed by a short wash with cold 0.5M NaCl PBS (high-salt wash) and a 5-min wash with cold PBS 0.5 M NaCl at 4°C. Finally, cells were washed again with cold PBS before collection.

RNA was recovered by direct lysis using the ML buffer (NucleoSpin miRNA kit, Macherey-Nagel, Dueren, Germany) spiked with 0.01 pmol of an internal control aptamer called M12-13, which refers to a generation of aptamers that utilizes a different set of primers for amplification (Sel1) than those used for EphA aptamer selection (Sel2). Recovered RNA was quantified by qRT-PCR using the Itaq Universal Sybr Green One Step Kit (Bio-Rad, Hercules, CA) and a LightCycler 489 II Thermal Cycler (Roche, Basel, Switzerland). All reactions were done in a 10-μL volume in triplicate.

The set of primers used were either the SEL2 set of primers or the SEL1 set of primers used for amplifying the aptamer reference control M12-13 (SEL1 FW: GGGGGAATTCTAATACGACTCACTATAGG GAGAGAGGAAGAGGGATGGG, SEL1 RV: GGGGGGATCCAG TACTATCGACCTCTGGGTTATG; SEL2 FW: TAATACGACTCA CTATAGGGAGGACGATGCGG, SEL2 RV: TCGGGCGAGTCGT CTG), or the SCR set of primers used to amplify the scramble sequence (SCR FW: ACCGAAAAAGACCTGGC, SCR RV: GGAAC GTAGACTTAGTATAG).

Samples were normalized to M12-23, as well as the PCR amplification efficiency of each aptamer relative to SCR aptamer. Fold change was obtained by applying the ΔΔCT mathematical model from Pfaffl.[69]

Sequences of the M12-23 aptamer used for normalization as well as the SCR and ATOP are shown in Table S3.

(2) Flow cytometry was used for selected sequences synthesized with a 5′-Cyan5 moiety (BioSpring, Frankfurt, Germany). For the binding assay performed to calculate the de-dissociation constant (K_D), resuspended cells (A673) were washed with BB (DPBS+/+ containing 100 μg/mL yeast tRNA and 100 μg/mL BSA) and counted. A total of 300,000 cells per point were incubated with the oligo sequence (ATOP or SCR) at a concentration ranging from 10 nM to 2 μM in 500 μL for 30 min at 37°C under mild agitation. Cells were washed twice, and bound aptamers were analyzed using a Gallios flow cytometer and Kaluza Analysis 2.1 software (Beckman Coulter, Brea, CA). Raw data can be found in Table S4. The fitting curve, in which the binding values in terms of MFI are plotted against the increasing concentration of radioligand, was designed using GraphPad Prism 7 after subtraction from the blank (MFI values of the SCR aptamer). The equilibrium binding constant was then calculated as the aptamer concentration needed to achieve a half-maximum binding at equilibrium [$Y = B_{max} \times X/(K_d + X)$].

For the internalization assay, 300,000 cells/well were seeded in a 6-well plate. Twenty-four hours after plating, cells were washed with serum-free medium and incubated with 100 μg/mL yeast tRNA in serum-free medium at 37°C for 15 min (blocking step). Cells were then incubated with the oligonucleotides for 2 h at 37°C. Unbound and surface-bound aptamers were removed by washing the cells twice with cold 0.5 M NaCl PBS (high-salt wash) before collection using trypsin. The internalized fraction was analyzed again using a Gallios flow cytometer and Kaluza Analysis 2.1 software (Beckman Coulter).

(3) Fluorescence microscopy: functionalization of the aptamer sequence with a Cy5 moiety was used to check for its localization within cells using a confocal microscope. Cells (A673) were plated on round coverslips (24-well plate) at a density of 75,000 cells per condition. The next day, medium was removed and cells were washed with incubation buffer serum-free medium containing yeast tRNA (100 mg/mL) at a concentration of 100 μg/mL to avoid non-specific binding. Aptamer was then added at a concentration of 400 nM and incubated for 6 h to allow for internalization before permeabilization and primary antibody incubation. Following the 6-h incubation period, cells were washed with PBS, fixed with cold PFA at 4% for 20 min at room temperature and washed again. Cells were then permeabilized, blocked, and incubated with the primary antibody overnight at 4°C. The next day, cells were washed, incubated with the secondary antibody, and finally mounted using ProlongGold antifade reagent with DAPI (Invitrogen, no. P36935). Cells were visualized at 60× using a Zeiss LSM 900 with an Airyscan 2 microscope (Zeiss, Oberkochen, Germany). Images were analyzed using Apeer software (Zeiss).

Western blot analysis

Cells were lysed with radioimmunoprecipitation assay buffer (RIPA buffer, Thermo Scientific) containing protease inhibitors (Complete Mini Protease Inhibitor Cocktail Tablets, Roche) and phosphatase inhibitors (PhosStop, Phosphatase Inhibitor Cocktail Tablets, Roche) by incubation for 30 min on ice. Samples were centrifuged at 13,000 × *g*, at 4°C, for 20 min and the protein content of the supernatants was determined using the Pierce BCA Protein Assay Kit (Thermo Scientific).

Lysate aliquots (≥40 μg) were resolved by 8%, 10%, 12%, or 15% SDS-PAGE (depending on protein molecular weight) and transferred to 0.2-μm pore nitrocellulose membranes (Bio-Rad). After blocking in a solution of 5% non-fat milk in 0.1% Tween PBS (PBS-T) at room temperature for 1 h, membranes were incubated overnight at 4°C with the primary antibody: EphA2 (Cell Signaling, no. 6997, Danvers, MA), phospho-EphA2 (Ser897) (Cell Signaling, no. 6347), p44/42 MAPK (Erk1/2) (Cell Signaling, no. 4695), Phospho-p44/42 MAPK (Erk1/2) (Thr202/Tyr204) (Cell Signaling, no. 4376), or α-tubulin (Sigma-Aldrich, no. T6199, St. Louis, MI). Blots were then incubated at room temperature for 1 h with a horseradish peroxidase-conjugated secondary antibody (1:2,000) and the peroxidase activity was detected by enhanced chemiluminescence (ECL WB

substrate, Thermo Scientific), following the manufacturer's instructions, in an Amersham Imager 600 (GE Healthcare). Immunodetection of β- and α-tubulin was used as a loading reference.

Pull-down assay

EphA2-expressing cells were cultured until confluence and collected. After washing with PBS, cell pellets were lysed directly using a cytoplasmatic extraction buffer (10 mM HEPES [pH 7.6], 60 mM KCl, 1 mM EDTA, 0.075% [v/v] NP40, 1 mM DTT, and protease/phosphatase inhibitors) and vortexed. The lysates (supernatant) were then collected after 5 min incubation on ice followed by a 5-min centrifugation at 1,500 rpm (cold centrifuge, 4°C). Protein concentration was quantified, and 500 μg of cell extracts incubated with 200 or 400 nM of biotinylated EphA2 aptamer or biotinylated scrambled aptamer in the presence of a non-specific competitor (yeast tRNA) at a final concentration of 100 μg/mL in a total volume of 500 μL (diluted in lysis buffer).

After 30 min incubation at room temperature on a rotating track, cell extracts were incubated for another 30 min in the presence of 50 μL of Dynabeads MyOne Streptavidin C1 (Invitrogen), previously washed twice with water and once in lysis buffer.

After incubation the supernatant was discarded and the beads were washed three times (5 min each wash) with lysis buffer. Bound proteins were eluted and denatured by adding 30 μL Laemmli buffer 3× (Bio-Rad) and heating at 100°C for 10 min. After 10 min centrifugation at 13,200 rpm, recovered proteins were subjected to SDS-PAGE (10%) western blot, with the input being represented by 10 μg of the whole-cell extract. Proteins were separated by electrophoresis and then blotted with anti EphA2 primary antibody (Cell Signaling).

Colony formation assay

A low number of cells (250 or 500 per well depending on the cell line) were plated in a 12-well plate and kept at 37°C with 5% CO_2. Aptamer treatment was performed at a concentration of 100 nM every 72 h starting 24 h after seeding. When colonies reached saturation (∼14 days after seeding), colonies were fixed with cold MetOH for 10 min and stained with crystal violet (Sigma-Aldrich) for 20 min. After washing and drying, images were taken and cells were bleached with 10% glacial acetic acid for 30 min to measure optical density of the solution at 570 nm using a Biotek PowerWave XS Microplate Reader (Marshal Scientific, Hampton, NH).

Migration assay

Migration was carried out following the Boyden chamber principle. Cells were pre-treated for 6 h with 250 nM of either ATOP or SCR. Cells were then trypsinized, resuspended in RPMI serum-free medium, and counted. Cells (150,000) in 150 μL serum-free medium were then plated into the upper side of a 24-well Transwell Permeable Support (Cultek, Madrid, Spain). FBS medium (10%) was placed on the lower side of the chamber and served as the chemoattractant for inducing migration. The same concentration of oligo was maintained in both sides of the chamber. Cells were incubated for 24 h. Cells that had migrated to the other side of the membrane were fixed with ethanol (EtOH) 70% and stained with crystal violet. Images of the membrane were taken using an Eclipse 80i (Nikon, Melville, NY) microscope. The percentage of migrated cells was evaluated by eluting crystal violet with 10% glacial acetic acid and reading the absorbance at 570 nm wavelength.

In vivo assay

(1) Aptamer treatment in an *in vivo* orthotopic mouse model: animal models for tumor growth or metastatic detection were performed as described by López-Alemany and Tirado.[47] Athymic nude mice were used (Hsd:Athymic Mide-Foxn1nu, Envigo, Indianapolis, IN). In brief, 1×10^6 A673 luciferin-labeled cells were resuspended in 0.1 mL PBS and injected into the gastrocnemius muscles of 6-week-old female mice. Mice were randomized into two groups (each n = 20) and were treated by i.v. injection of aptamers, ATOP or SCR, 20 nmol/mice (1.6 mg/kg) after cell inoculation every 3 days from day 1 until day 22. The growth of primary tumors was monitored by periodic measurements of the limb using a caliper. Tumor volume was calculated according to the formula $(L \times l^2/2)$, where L is the longer diameter and l the shorter diameter. The inoculated animals were monitored *in vivo* every week by bioluminescence imaging. Anesthetized mice were injected intraperitoneally with D-luciferin (150 mg/kg, Caliper Life Science, Hopkinton, M) and imaged with 1-min acquisition times using an IVIS Luminar XR System Apparatus (Perkin Elmer, Waltham, MA). Once primary tumor-bearing limbs reached a critical volume (800 mm^3), 15–20 days after inoculation, gastrocnemius muscles were surgically resected. Mice were maintained anesthetized with a 2% isoflurane/5% O_2 mixture during all surgical procedures in an anesthesia apparatus (Vet-Tecnic, Barcelona, Spain). Injuries were sealed using a TB10 silk suture (B. Braun, Germany). After surgery, the formation of lung metastases was monitored by weekly *in vivo* IVIS readings. At the endpoint of the experiment, mice were euthanized, lungs were harvested, and an *ex vivo* IVIS reading was performed. Primary tumors and lungs were fixed in 4% buffered paraformaldehyde for histopathological analysis. Mice were cared for according to the Institutional Guidelines for the Care and Use of Laboratory Animals. Ethics approval was provided by Catalan Government Animal Care Committee (permit no. 9745).

(2) Aptamer biodistribution: mice were injected with 5×10^5 A673 luciferin-labeled cells as described above. Tumor growth was monitored and, when the tumor-bearing limb reached a critical volume (800 mm^3), mice were randomly divided into two groups and treated with a single i.v. injection of fluorescent-labeled aptamers with cyanine 7 (Cy7): Cy7-ATOP or Cy7-SCR at a concentration of 1.6 mg/kg. Fluorescence of *in vivo* whole mice was read at 30 min, and at 1, 2, 8, 24, and 78 h, using IVIS (λ excitation = 740 nm and λ emission = 800 nm). After 72 h of aptamer injection, mice were euthanized and *ex vivo* fluorescence in tumor, heart, liver, kidneys, and spleen was measured.

DATA AVAILABILITY

All data generated or analyzed during this study are included in this published article and its supplemental information files.

SUPPLEMENTAL INFORMATION

Supplemental information can be found online at https://doi.org/10.1016/j.omtn.2023.05.003.

ACKNOWLEDGMENTS

We would like to thank Saioa Mendizurri Sanchez from the Bioimaging Platform and Jose M.A. Vaquero, manager of the Flow Cytometry Platform of the IDIBELL Scientific and Technical Services for their support with the confocal imaging and FACS analysis respectively. This work was supported by the following grants: Instituto de Salud Carlos III and-FEDER (CES12/021, PI11/00038, PI15/00035), Ministerio de Ciencia e Innovación (RTI2018-094787-B-I00, PID2021-122828OB-I00), AGAUR (2017SGR332), Asociación Española Contra el Cáncer (IDEAS18012MART, INNO20011MART), CERCA Program/Generalitat de Catalunya, Fundación Alba Pérez lucha contra el cáncer infantil (to O.M.T.). National Institutes of Health (R01CA138503), Mary Kay Foundation (9033-12 and 001-09), and the Roy J Carver Charitable Trust (RJCCT 01-224) (to P.H.G.). AHA Scientist Development Grant (14SDG18850071) and NHLBI R01 (HL139581-01A1) (to W.H.T.). Fundación Alba Pérez lucha contra el cáncer infantile (to S.G.-M.).

AUTHOR CONTRIBUTIONS

Conceptualization, O.M.T., P.H.G., W.H.T., and L.S.-V.; methodology, L.S.-V. and R.L.-A.; investigation, L.S.-V., J.P.D., K.T., W.H.T., D.D., P.H.G., S.G.-M., M.C.-B., M.R.-L., S.S.-S., M.P.-C., L.d.P., R.L.-A., and S.M.-M.; writing – original draft, L.S.-V.; writing –review & editing, L.S.-V., R.L.-A., O.M.T., and P.H.G.; visualization, L.S.-V.; funding acquisition, O.M.T., W.H.T., and P.H.G.; software, W.H.T.

DECLARATION OF INTERESTS

O.M.T. is founder of Aptadel Therapeutics and has shares. P.H.G is an employee of Wave Life Sciences.

REFERENCES

1. Thaker, P.H., Deavers, M., Celestino, J., Thornton, A., Fletcher, M.S., Landen, C.N., Kinch, M.S., Kiener, P.A., and Sood, A.K. (2004). EphA2 expression is associated with aggressive features in ovarian carcinoma. Clin. Cancer Res. *10*, 5145–5150.
2. Lin, Y.G., Han, L.Y., Kamat, A.A., Merritt, W.M., Landen, C.N., Deavers, M.T., Fletcher, M.S., Urbauer, D.L., Kinch, M.S., and Sood, A.K. (2007). EphA2 overexpression is associated with angiogenesis in ovarian cancer. Cancer *109*, 332–340.
3. Walker-Daniels, J., Coffman, K., Azimi, M., Rhim, J.S., Bostwick, D.G., Snyder, P., Kerns, B.J., Waters, D.J., and Kinch, M.S. (1999). Overexpression of the EphA2 tyrosine kinase in prostate cancer. Prostate *41*, 275–280.
4. Zhao, Y., Cai, C., Zhang, M., Shi, L., Wang, J., Zhang, H., Ma, P., and Li, S. (2021). Ephrin-A2 promotes prostate cancer metastasis by enhancing angiogenesis and promoting EMT. J. Cancer Res. Clin. Oncol. *147*, 2013–2023.
5. Duxbury, M.S., Ito, H., Zinner, M.J., Ashley, S.W., and Whang, E.E. (2004). EphA2: a determinant of malignant cellular behavior and a potential therapeutic target in pancreatic adenocarcinoma. Oncogene *23*, 1448–1456.
6. Wykosky, J., Gibo, D.M., Stanton, C., and Debinski, W. (2005). EphA2 as a novel molecular marker and target in glioblastoma multiforme. Mol. Cancer Res. *3*, 541–551.
7. Wang, L.F., Fokas, E., Bieker, M., Rose, F., Rexin, P., Zhu, Y., Pagenstecher, A., Engenhart-Cabillic, R., and An, H.X. (2008). Increased expression of EphA2 correlates with adverse outcome in primary and recurrent glioblastoma multiforme patients. Oncol. Rep. *19*, 151–156.
8. Kinch, M.S., Moore, M.-B., and Harpole, D.H. (2003). Predictive value of the EphA2 receptor tyrosine kinase in lung cancer recurrence and survival. Clin. Cancer Res. *9*, 613–618.
9. Margaryan, N.v., Strizzi, L., Abbott, D.E., Seftor, E.A., Rao, M.S., Hendrix, M.J.C., and Hess, A.R. (2009). EphA2 as a promoter of melanoma tumorigenicity. Cancer Biol. Ther. *8*, 279–288.
10. Udayakumar, D., Zhang, G., Ji, Z., Njauw, C.N., Mroz, P., and Tsao, H. (2011). Epha2 is a critical oncogene in melanoma. Oncogene *30*, 4921–4929.
11. Miyazaki, T., Kato, H., Fukuchi, M., Nakajima, M., and Kuwano, H. (2003). EphA2 overexpression correlates with poor prognosis in esophageal squamous cell carcinoma. Int. J. Cancer *103*, 657–663.
12. Dunne, P.D., Dasgupta, S., Blayney, J.K., McArt, D.G., Redmond, K.L., Weir, J.A., Bradley, C.A., Sasazuki, T., Shirasawa, S., Wang, T., et al. (2016). EphA2 expression is a key driver of migration and invasion and a poor prognostic marker in colorectal cancer. Clin. Cancer Res. *22*, 230–242.
13. Kataoka, H., Igarashi, H., Kanamori, M., Ihara, M., Wang, J.D., Wang, Y.J., Li, Z.Y., Shimamura, T., Kobayashi, T., Maruyama, K., et al. (2004). Correlation of EPHA2 overexpression with high microvessel count in human primary colorectal cancer. Cancer Sci. *95*, 136–141.
14. Saito, T., Masuda, N., Miyazaki, T., Kanoh, K., Suzuki, H., Shimura, T., Asao, T., and Kuwano, H. (2004). Expression of EphA2 and E-cadherin in colorectal cancer: correlation with cancer metastasis. Oncol. Rep. *11*, 605–611.
15. Giordano, G., Merlini, A., Ferrero, G., Mesiano, G., Fiorino, E., Brusco, S., Centomo, M.L., Leuci, V., D'ambrosio, L., Aglietta, M., et al. (2021). EphA2 expression in bone sarcomas: bioinformatic analyses and preclinical characterization in patient-derived models of osteosarcoma, ewing's sarcoma and chondrosarcoma. Cells *10*, 2893.
16. Posthumadeboer, J., Piersma, S.R., Pham, T.v., van Egmond, P.W., Knol, J.C., Cleton-Jansen, A.M., van Geer, M.A., van Beusechem, V.W., Kaspers, G.J.L., van Royen, B.J., et al. (2013). Surface proteomic analysis of osteosarcoma identifies EPHA2 as receptor for targeted drug delivery. Br. J. Cancer *109*, 2142–2154.
17. Zhang, X. (2021). The expression profile and prognostic values of EPHA family members in breast cancer. Front. Oncol. *11*, 619949.
18. Brantley-Sieders, D.M., Zhuang, G., Hicks, D., Fang, W.B., Hwang, Y., Cates, J.M.M., Coffman, K., Jackson, D., Bruckheimer, E., Muraoka-Cook, R.S., and Chen, J. (2008). The receptor tyrosine kinase EphA2 promotes mammary adenocarcinoma tumorigenesis and metastatic progression in mice by amplifying ErbB2 signaling. J. Clin. Invest. *118*, 64–78.
19. Zelinski, D.P., Zantek, N.D., Stewart, J.C., Irizarry, A.R., and Kinch, M.S. (2001). EphA2 overexpression causes tumorigenesis of mammary epithelial cells. Cancer Res. *61*, 2301–2306.
20. Brantley-Sieders, D.M., Fang, W.B., Hicks, D.J., Zhuang, G., Shyr, Y., and Chen, J. (2005). Impaired tumor microenvironment in EphA2-deficient mice inhibits tumor angiogenesis and metastatic progression. Faseb. J. *19*, 1884–1886.
21. Wilson, K., Shiuan, E., and Brantley-Sieders, D.M. (2021). Oncogenic functions and therapeutic targeting of EphA2 in cancer. Oncogene *40*, 2483–2495.
22. Coffman, K.T., Hu, M., Carles-Kinch, K., Tice, D., Donacki, N., Munyon, K., Kifle, G., Woods, R., Langermann, S., Kiener, P.A., and Kinch, M.S. (2003). Differential EphA2 epitope display on normal versus malignant cells. Cancer *63*, 7907–7912.
23. Kinch, M.S., and Carles-Kinch, K. (2003). Overexpression and functional alterations of the EphA2 tyrosine kinase in cancer. Clin. Exp. Metastasis *20*, 59–68.
24. Miao, H., Li, D.Q., Mukherjee, A., Guo, H., Petty, A., Cutter, J., Basilion, J.P., Sedor, J., Wu, J., Danielpour, D., et al. (2009). EphA2 mediates ligand-dependent inhibition and ligand-independent promotion of cell migration and invasion via a reciprocal regulatory loop with akt. Cancer Cell *16*, 9–20.
25. Garcia-Monclús, S., López-Alemany, R., Almacellas-Rabaiget, O., Herrero-Martín, D., Huertas-Martinez, J., Lagares-Tena, L., Alba-Pavón, P., Hontecillas-Prieto, L., Mora, J., de Álava, E., et al. (2018). EphA2 receptor is a key player in the metastatic onset of Ewing sarcoma. Int. J. Cancer *143*, 1188–1201.
26. Carles-Kinch, K., Kilpatrick, K.E., Stewart, J.C., and Kinch, M.S. (2002). Antibody targeting of the EphA2 tyrosine kinase inhibits malignant cell behavior. Cancer Res. *62*, 2840–2847.

27. Yang, Y., Nian, S., Li, L., Wen, X., Liu, Q., Zhang, B., Lan, Y., Yuan, Q., and Ye, Y. (2021). Fully human recombinant antibodies against EphA2 from a multi-tumor patient immune library suitable for tumor-targeted therapy. Bioengineered *12*, 10379–10400.

28. Biao-xue, R., Xi-guang, C., Shuan-ying, Y., Wei, L., and Zong-juan, M. (2011). EphA2-Dependent molecular targeting therapy for malignant tumors. Curr. Cancer Drug Targets *11*, 1082–1097.

29. Jackson, D., Gooya, J., Mao, S., Kinneer, K., Xu, L., Camara, M., Fazenbaker, C., Fleming, R., Swamynathan, S., Meyer, D., et al. (2008). A human antibody-drug conjugate targeting EphA2 inhibits tumor growth in vivo. Cancer Res. *68*, 9367–9374.

30. Koolpe, M., Dail, M., and Pasquale, E.B. (2002). An ephrin mimetic peptide that selectively targets the EphA2 receptor. J. Biol. Chem. *277*, 46974–46979.

31. Wang, S., Placzek, W.J., Stebbins, J.L., Mitra, S., Noberini, R., Koolpe, M., Zhang, Z., Dahl, R., Pasquale, E.B., and Pellecchia, M. (2012). Novel targeted system to deliver chemotherapeutic drugs to EphA2-expressing cancer cells. J. Med. Chem. *55*, 2427–2436.

32. Stoltenburg, R., Reinemann, C., and Strehlitz, B. (2007). SELEX—a (r)evolutionary method to generate high-affinity nucleic acid ligands. Biomol. Eng. *24*, 381–403.

33. Odeh, F., Nsairat, H., Alshaer, W., Ismail, M.A., Esawi, E., Qaqish, B., Bawab, A.A., Ismail, S.I., and Jo, A.A.B. (2019). Aptamers chemistry: chemical modifications and conjugation strategies. Molecules *25*, 3.

34. Ng, E.W.M., Shima, D.T., Calias, P., Cunningham, E.T., Guyer, D.R., and Adamis, A.P. (2006). Pegaptanib, a targeted anti-VEGF aptamer for ocular vascular disease. Nat. Rev. Drug Discov. *5*, 123–132.

35. Morita, Y., Leslie, M., Kameyama, H., Volk, D.E., and Tanaka, T. (2018). Aptamer therapeutics in cancer: current and future. Cancers *10*, 80.

36. Kovacevic, K.D., Gilbert, J.C., and Jilma, B. (2018). Pharmacokinetics, pharmacodynamics and safety of aptamers. Adv. Drug Deliv. Rev. *134*, 36–50.

37. Hernández-Jiménez, M., Martín-Vílchez, S., Ochoa, D., Mejía-Abril, G., Román, M., Camargo-Mamani, P., Luquero-Bueno, S., Jilma, B., Moro, M.A., Fernández, G., et al. (2022). First-in-human phase I clinical trial of a TLR4-binding DNA aptamer, ApTOLL: safety and pharmacokinetics in healthy volunteers. Mol. Ther. Nucleic Acids *28*, 124–135.

38. Fu, Z., and Xiang, J. (2020). Aptamers, the nucleic acid antibodies, in cancer therapy. Int. J. Mol. Sci. *21*, 2793.

39. Halama, N., Prüfer, U., Froemming, A., Beyer, D., Eulberg, D., Jungnelius, J.U., and Mangasarian, A. (2019). Phase I/II study with CXCL12 inhibitor NOX-A12 and pembrolizumab in patients with microsatellite-stable, metastatic colorectal or pancreatic cancer. Ann. Oncol. *30*, v231.

40. Tuerk, C., and Gold, L. (1990). Systematic evolution of ligands by exponential enrichment: RNA ligands to bacteriophage T4 DNA polymerase. Science *249*, 505–510.

41. Catuogno, S., and Esposito, C.L. (2017). Aptamer cell-based selection: overview and advances. Biomedicines *5*, 49.

42. Thiel, W.H., and Giangrande, P.H. (2016). Analyzing HT-SELEX data with the Galaxy Project tools–A web based bioinformatics platform for biomedical research. Methods *97*, 3–10.

43. Thiel, W.H., Bair, T., Peek, A.S., Liu, X., Dassie, J., Stockdale, K.R., Behlke, M.A., Miller, F.J., and Giangrande, P.H. (2012). Rapid identification of cell-specific, internalizing RNA aptamers with bioinformatics analyses of a cell-based aptamer selection. PLoS One *7*, e43836.

44. Lorenz, R., Bernhart, S.H., Höner Zu Siederdissen, C., Tafer, H., Flamm, C., Stadler, P.F., and Hofacker, I.L. (2011). ViennaRNA package 2.0. Algorithm Mol. Biol. *6*, 26.

45. Fontana, W., Konings, D.A., Stadler, P.F., and Schuster, P. (1993). Statistics of RNA secondary structures. Biopolymers *33*, 1389–1404.

46. Shannon, P., Markiel, A., Ozier, O., Baliga, N.S., Wang, J.T., Ramage, D., Amin, N., Schwikowski, B., and Ideker, T. (2003). Cytoscape: a software environment for integrated models of biomolecular interaction networks. Genome Res. *13*, 2498–2504.

47. López-Alemany, R., and Tirado, O.M. (2021). Metastasis assessment in ewing sarcoma using orthotopic xenografts. Methods Mol. Biol. *2226*, 201–213.

48. Kulbachinskiy, A.v. (2007). Methods for selection of aptamers to protein targets. Biochemistry *72*, 1505–1518.

49. Thiel, W.H., Thiel, K.W., Flenker, K.S., Bair, T., Dupuy, A.J., McNamara, J.O., 2nd, Miller, F.J., and Giangrande, P.H. (2015). Cell-internalization SELEX: method for identifying cell-internalizing RNA aptamers for delivering siRNAs to target cells. Methods Mol. Biol. *1218*, 187–199.

50. Sun, H., Zhu, X., Lu, P.Y., Rosato, R.R., Tan, W., and Zu, Y. (2014). Oligonucleotide aptamers: new tools for targeted cancer therapy. Mol. Ther. Nucleic Acids *3*, e182.

51. Zumrut, H.E., and Mallikaratchy, P.R. (2020). Ligand guided selection (LIGS) of artificial nucleic acid ligands against cell surface targets. ACS Appl. Bio Mater. *3*, 2545–2552.

52. Affinito, A., Quintavalle, C., Esposito, C.L., Roscigno, G., Giordano, C., Nuzzo, S., Ricci-Vitiani, L., Scognamiglio, I., Minic, Z., Pallini, R., et al. (2020). Targeting ephrin receptor tyrosine kinase A2 with a selective aptamer for glioblastoma stem cells. Mol. Ther. Nucleic Acids *20*, 176–185.

53. Chen, Y., Cao, A., Li, Q., and Quan, J. (2022). Identification of DNA aptamers that specifically targets EBV+ nasopharyngeal carcinoma via binding with EphA2/CD98hc complex. Biochem. Biophys. Res. Commun. *608*, 135–141.

54. Wykosky, J., Gibo, D.M., Stanton, C., and Debinski, W. (2008). Interleukin-13 receptor alpha 2, EphA2, and Fos-related antigen 1 as molecular denominators of high-grade astrocytomas and specific targets for combinatorial therapy. Clin. Cancer Res. *14*, 199–208.

55. Zeng, G., Hu, Z., Kinch, M.S., Pan, C.X., Flockhart, D.A., Kao, C., Gardner, T.A., Zhang, S., Li, L., Baldridge, L.A., et al. (2003). High-level expression of EphA2 receptor tyrosine kinase in prostatic intraepithelial neoplasia. Am. J. Pathol. *163*, 2271–2276.

56. Mudali, S.v., Fu, B., Lakkur, S.S., Luo, M., Embuscado, E.E., and Iacobuzio-Donahue, C.A. (2006). Patterns of EphA2 protein expression in primary and metastatic pancreatic carcinoma and correlation with genetic status. Clin. Exp. Metastasis *23*, 357–365.

57. Hafner, C., Schmitz, G., Meyer, S., Bataille, F., Hau, P., Langmann, T., Dietmaier, W., Landthaler, M., and Vogt, T. (2004). Differential gene expression of eph receptors and ephrins in benign human tissues and cancers. Clin. Chem. *50*, 490–499.

58. Singh, D.R., Kanvinde, P., King, C., Pasquale, E.B., and Hristova, K. (2018). The EphA2 receptor is activated through induction of distinct, ligand-dependent oligomeric structures. Commun. Biol. *1*, 15.

59. Bumcrot, D., Manoharan, M., Koteliansky, V., and Sah, D.W.Y. (2006). RNAi therapeutics: a potential new class of pharmaceutical drugs. Nat. Chem. Biol. *2*, 711–719.

60. Roberts, T.C., Langer, R., and Wood, M.J.A. (2020). Advances in oligonucleotide drug delivery. Nat. Rev. Drug Discov. *19*, 673–694.

61. Kruspe, S., and Giangrande, P.H. (2017). Aptamer-siRNA chimeras: Discovery, progress, and future prospects. Biomedicines *5*, 45.

62. Yang, Y., Wang, S., Ma, P., Jiang, Y., Cheng, K., Yu, Y., Jiang, N., Miao, H., Tang, Q., Liu, F., et al. (2023). Drug conjugate-based anticancer therapy - current status and perspectives. Cancer Lett. *552*, 215969.

63. Bode, S.A., and Löwik, D.W.P. (2017). Constrained cell penetrating peptides. Drug Discov. Today Technol. *26*, 33–42.

64. Xiang, D., Zheng, C., Zhou, S.F., Qiao, S., Tran, P.H.L., Pu, C., Li, Y., Kong, L., Kouzani, A.Z., Lin, J., et al. (2015). Superior performance of aptamer in tumor penetration over antibody: implication of aptamer-based theranostics in solid tumors. Theranostics *5*, 1083–1097.

65. Ellington, A.D., and Szostak, J.W. (1990). In vitro selection of RNA molecules that bind specific ligands. Nature *346*, 818–822.

66. Thiel, K.W., Hernandez, L.I., Dassie, J.P., Thiel, W.H., Liu, X., Stockdale, K.R., Rothman, A.M., Hernandez, F.J., McNamara, J.O., and Giangrande, P.H. (2012). Delivery of chemo-sensitizing siRNAs to HER2+-breast cancer cells using RNA aptamers. Nucleic Acids Res. *40*, 6319–6337.

67. Hernandez, F.J., Kalra, N., Wengel, J., and Vester, B. (2009). Aptamers as a model for functional evaluation of LNA and 2'-amino LNA. Bioorg. Med. Chem. Lett. *19*, 6585–6587.

68. Hernandez, F.J., Dondapati, S.K., Ozalp, V.C., Pinto, A., O'Sullivan, C.K., Klar, T.A., and Katakis, I. (2009). Label free optical sensor for Avidin based on single gold nanoparticles functionalized with aptamers. J. Biophot. *2*, 227–231.

69. Pfaffl, M.W. (2001). A new mathematical model for relative quantification in real-time RT-PCR. Nucleic Acids Res. *29*, e45.